

**JOHANNES KEPLER  
UNIVERSITY LINZ**

Submitted by

**Elisabeth Leeb**

Submitted at

**Institute of Physical  
Chemistry and Linz Institute  
of Organic Solar Cells**

Supervisor

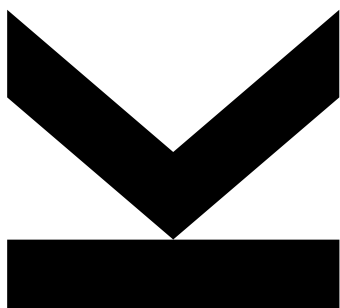
**Assoc. Prof.  
DI Dr. Markus Clark  
Scharber**

Co-Supervisor

**Dr.<sup>in</sup> Yolanda Salinas**

September 2020

# **SYNTHESIS OPTIMIZATION OF LEAD BROMIDE PEROVSKITE NANOPARTICLES**



Bachelor Thesis

to obtain the academic degree of

Bachelor of Science (BSc)

in the Bachelor's Program

Chemistry and Chemical Technology

**JOHANNES KEPLER  
UNIVERSITY LINZ**

Altenberger Str. 69  
4040 Linz, Austria  
www.jku.at  
DVR 0093696

## STATUTORY DECLARATION

I hereby declare that the thesis submitted is my own unaided work, that I have not used any sources other than those indicated and that all direct and indirect sources are acknowledged as references.

This printed thesis is identical with the electronically submitted version.

Place, Date

Signature

## Acknowledgement

First and foremost I would like to thank o. Univ. Prof. Mag. Dr.DDr. h.c. Niyazi Serdar Sariciftci for introducing me to the Linzer Institute of Organic Solar Cells and for giving me the opportunity to work amongst this group of kind, knowledgeable and supportive people.

I would also like to thank Univ. Prof. Dr. Oliver Brüggemann for offering me the use of his laboratory. Special thanks also to the whole team of the Institute of Polymer Chemistry for their kindness and swift help with every problem at hand.

My biggest thanks go out to my supervisor Assoc. Prof. DI Dr. Markus Scharber for his guidance within this work and seemingly unending patience with all of my questions. It was a real pleasure being able to learn so much.

Additionally, I would like to express my deepest gratitude to my Co-supervisor Dr.<sup>in</sup> Yolanda Salinas for all her encouragement and all the time spent discussing the latest results.

A special thank you to DI Dominik Wielend, who with his infectious curiosity and enthusiasm developed my interest in physical chemistry as well as my friends Magdalena Fidler and Nadine Kleinbruckner for proof-reading several versions of this thesis and for thoroughly improving upon my time spent at the University. Furthermore, I would like to thank the whole LIOS team for always providing support and ideas whenever they might be needed.

Last but not least, I would like to thank my parents for their continuing support of my studies as well as my stepdad Robert for always showing interest in my shiny green particles.

## Abstract

Perovskite nanoparticles (PNPs) with high photoluminescence quantum yields (PLQYs) and tuneable band gaps are of great interest for various applications. Fine tuning the size and emission maximum has been achieved through different approaches. The aim of this thesis was to optimize the synthesis of lead bromide based perovskites, in order to achieve a reliable method of production. Two different compositions of nanoparticles were examined, one being methylammonium lead bromide ( $\text{MAPbBr}_3$ ) and the other being formamidinium lead bromide ( $\text{FAPbBr}_3$ ). The focus has been laid on providing a reliable method of synthesis for these nanoparticles using a ligand assisted precipitation method. The ligands used in this thesis were boc-lysine and hexanoic acid. Thin films were produced by centrifugal casting of the resulting colloidal solution onto glass substrates.

The addition of water to the precursor solution was used to maximize the PLQY, with the most favourable results being achieved by adding 16 mol. equivalences of water. Moreover, the effect of aging of the precursor on the resulting nanoparticle has been studied. Here, one day has been identified as the ideal age of the precursor solution. Using those parameters, it was possible to produce PNPs with PLQYs of close to 100%. The mean values were 516 nm ( $\text{MAPbBr}_3$ ) and 536 nm ( $\text{FAPbBr}_3$ ). Additionally, the different behaviour of the two compositions has been thoroughly studied.

These results conclude in the potential application of PNPs in optoelectronic devices, such as LEDs.

## Kurzfassung

Perowskit-Nanopartikel (PNPs) mit einer hohen Photolumineszenz-Quantenausbeute (PLQY) und einer einstellbaren Bandlücke zeigen großes Potential für verschiedene Anwendungen. Die Feinanpassung von Größe und Emissionsmaximum wurde bereits durch verschiedene Methoden erzielt. Das Ziel dieser Arbeit war die Optimierung der Synthese von Perowskiten, die auf Bleibromid basieren, um eine verlässliche Methode für deren Synthese bereitzustellen. Dazu wurden zwei verschiedenen Zusammensetzungen an Nanopartikel untersucht, Methylammoniumbleibromid ( $\text{MAPbBr}_3$ ) und Formamidiniumbleibromid ( $\text{FAPbBr}_3$ ). Der Schwerpunkt dieser Arbeit lag auf der Entwicklung einer verlässlichen Synthesemethode der Nanopartikel, wofür eine ligandenunterstützte Fällungsmethode genutzt wurde. Die in dieser Arbeit verwendeten Liganden waren boc-Lysin und Capronsäure. Zur Herstellung von Dünnschichtfilmen wurde die dabei entstehende kolloide Lösung mittels Zentrifugalbeschichtung auf Glasträger aufgetragen.

Die Zugabe von Wasser zur Vorläuferlösung wurde genutzt, um die PLQYs zu maximieren, wobei die besten Resultate bei der Zugabe von 16 mol. Äquivalenten Wasser erzielt wurden. Darüber hinaus wurde der Effekt des Alters der Vorläuferlösung auf die resultierenden Nanopartikeln untersucht. Hierbei wurde ein Tag als ideales Alter für die Vorläuferlösung identifiziert. Unter Verwendung dieser Parameter war es möglich, PNPs mit einer PLQY von knapp 100% zu erzeugen. Die Emissionsmaxima lagen hier bei rund 516 nm ( $\text{MAPbBr}_3$ ) und 536 nm ( $\text{FAPbBr}_3$ ). Darüber hinaus wurde das unterschiedliche Verhalten der beiden Zusammensetzungen der PNPs eingehend untersucht.

Diese Ergebnisse zeigen ein großes Potential der PNPs in der Anwendung in optoelektronischen Geräten, wie zum Beispiel LEDs.

# TABLE OF CONTENTS

1. Introduction .....	7
1.1. Perovskite materials .....	7
1.2. Quantum Confinement .....	11
1.3. Photoluminescence .....	13
2. Experimental .....	13
2.1. Precursor Solutions .....	13
2.2. Thin Films .....	14
2.3. Colloidal Solutions .....	14
3. Results and Discussion.....	14
3.1. Organic Component .....	14
3.2. Water Content .....	18
3.2.1. Additive to Precursor .....	18
3.2.2. Ambient Humidity .....	19
3.2.3. Solvent .....	20
3.3. Methanol Addition to Precursor Solution .....	21
3.4. Age of Precursor.....	22
3.5. Low Temperature Spectroscopy.....	23
3.5.1. MAPbBr <sub>3</sub> Thin Film .....	23
3.5.2. FAPbBr <sub>3</sub> Thin Film.....	25
4. Conclusion .....	26
5. Appendix .....	26
5.1. Chemicals.....	26
5.2. Instruments.....	27
6. Literature.....	28

# 1. Introduction

Metal halide perovskite nanostructures have emerged in recent decades in various applications. The appeal of those nanostructures lies in their high photoluminescence quantum yields (PLQY) as well as their tuneable emission maximum, contributed with their low cost and easy processability. They show great promise for applications such as solar cells with efficiencies up to 20%<sup>[1]</sup>, photodetectors<sup>[2]</sup>, photocatalysts<sup>[3]</sup> as well as highly efficient light emitting diodes<sup>[4]</sup>.

The aim of this work was to produce lead halide perovskite nanoparticles, with high PLQYs and an emission maximum of above 500 nm. The nanoparticles have been characterized mainly in the form of thin films deposited on glass substrates as well as in the form of colloidal solutions, with the effect of the water content within the perovskite structure being the main focus of this thesis. Additionally, the composition of the nanoparticles has been varied, with both methylammonium bromide and formamidinium bromide used as the organic component.

## 1.1. Perovskite materials

Perovskite materials are defined by their crystal structure, with their name derived from the first discovered mineral with perovskite structure. The typical structure of perovskite materials is  $ABX_3$ , with A being a monovalent cation, B a divalent cation and X a halide anion, with the cations being of vastly different sizes. As can be seen in **Figure 1**, the B cations are coordinated with the X anion forming a cubic structure<sup>[5]</sup>. The A cations fill the space between the connected octahedral structures and neutralize the charged complex. By varying the composition of the perovskite, different optical properties can be reached due to the change in band gap<sup>[6]</sup>.

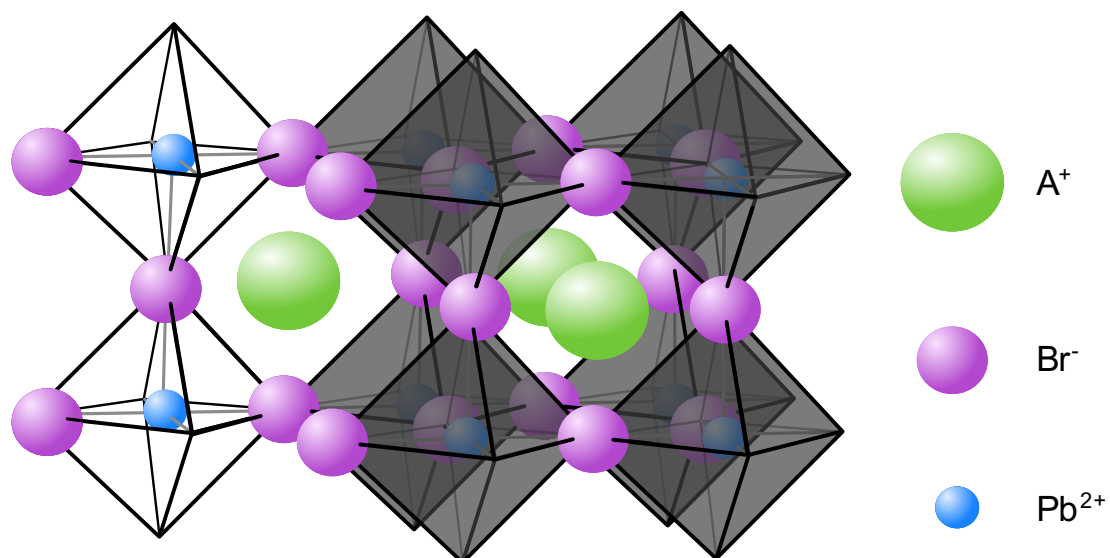


**Figure 1:** Schematic depiction of the general perovskite structure.

Two types of perovskites can be differentiated, either fully inorganic or hybrid perovskite structures. In inorganic perovskites structures, the A cation is an inorganic atom, while in hybrid perovskites the position of the A cation is filled with an organic molecule. This molecule has to be small enough to fit within the confined space between the octahedral structures, only consisting of three or less carbon-carbon or carbon-nitrogen bonds if a three-dimensional structure is to be achieved. The incorporation of organic molecules within the perovskite structure reduces the symmetry of the crystal formed<sup>[7]</sup>.

The Goldschmidt tolerance factor (**Eq. 1**) is a widely used parameter to characterize the geometric stability as well as the disorientation within the perovskite crystal structure. It is defined by the ratio of the ionic radii, with ideal perovskite structures displaying a factor of 1. If the ratio is not 1, the crystallite structure deviates from this ideal closely packed cubic structure, resulting in higher geometric strain and crystal distortion<sup>[8]</sup>. The larger the deviation, the greater the distortion as well as the resulting instability of the crystal structure. Materials with a Goldschmidt tolerance factor lower than 0.77 and higher than 1.05 no longer display a perovskite structure<sup>[9]</sup>.

$$t = \frac{r_A + r_X}{\sqrt{2} (r_B + r_X)} \quad (\text{Eq. 1})$$

with:  $r_A$  = radius of A cation

$r_B$  = radius of B cation

$r_X$  = radius of halide anion

When synthesizing PNPs, a widely used method is the ligand-assisted precipitation method due to its convenient reaction conditions, easy implementation and low cost. Surface ligands are used to influence crystal growth termination and are therefore vital for PLQYs as well as the final stability of the structure. The organic ligands commonly used during synthesis of inorganic nanoparticles tend to be rather large and therefore, hinder the inter-particle coupling. This in turn impedes the charge transport. In order to bypass this problem, the most used surfactants during the synthesis of PNPs are carboxylic acids with a carbon-chain no longer than 20 carbon atoms, which are paired with an amine<sup>[10]</sup>. These surfactants should hinder the aggregation of the nanoparticles within the solution and further the assembly of tightly packed thin films while also being conducive to charge conductivity.

Various carboxylic acids have been used as surface ligand for PNPs such as oleic, decanoic, octanoic, hexanoic and propanoic acid, with the size of the acid equally influencing the size of the PNPs. When using 2-adamantylammonium bromide, which is commonly used as the second surface ligand, propionic acid has shown the least tendency to aggregate within the solution<sup>[11]</sup>. However, in the place of 2-adamantylammonium bromide, a suitable amino

acid can also be implemented, such as the proteinogenic essential amino acid L-lysine. As those amino acids provide both a negatively and positively charged group, one molecule can passivate defects within the crystal structure caused by both  $\text{Pb}^{2+}$  or  $\text{Br}^-$ . However, in order to ensure selective orientation of the amino acid, the  $\alpha$ -amino group needs to be blocked, so that only the primary amine is used in passivating the surface. This is done, by equipping the  $\alpha$ -amino group with a protecting group, specifically *tert*-butyloxycarbonyl (boc). Additionally, preserving the  $\alpha$ -amino group would leave the possibility open of further functionalizing the PNPs by modification of this group<sup>[12]</sup>. For the carboxylic acid, hexanoic acid (HeA) showed the most promising result in combination with boc-lysine. HeA is used to protonate the amino acid, therefore increasing the number of charged groups capable of passivating the PNP surface<sup>[12]</sup>, as seen in **Figure 2**.

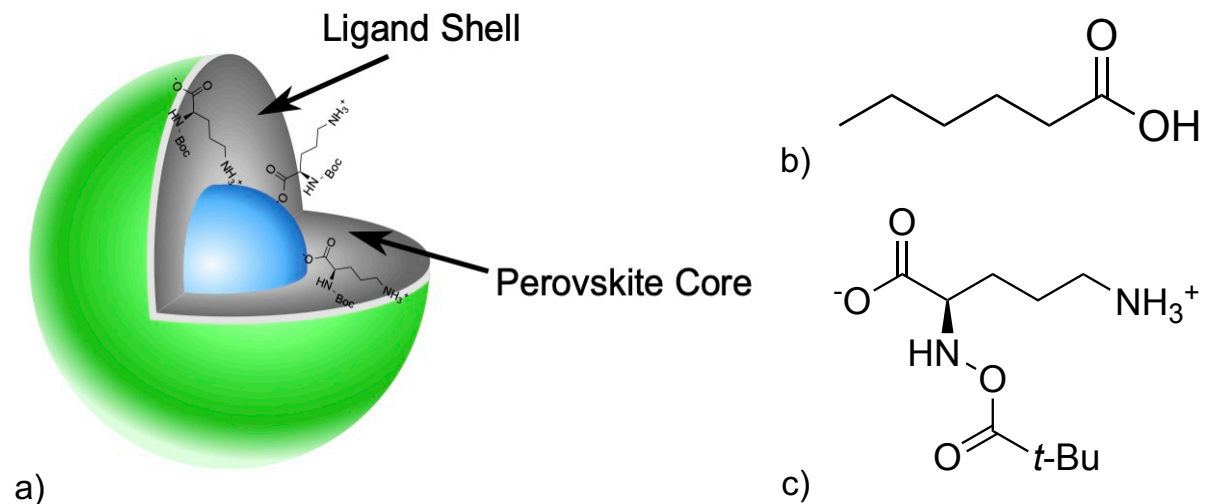


**Figure 2:** a) Perovskite core with capping agents and molecular structure of b) hexanoic acid and c) *tert*-butyloxycarbonyl lysine.

As a final product of this ligand-assisted precipitation method, a colloidal solution containing the nanoparticles is obtained. This solution can be further processed to thin films. A prominent method of nanoparticle deposition is spin coating<sup>[13]</sup>, where a small amount of product is applied on the center of a flat substrate. Further on, the substrate is rotated, spreading the coating material using the centrifugal force. However, this method can lead to a film thinning in the center of the substrate and an accumulation of product around the edge. In contrast, centrifugal casting has been shown to produce more even films across the substrate. As can be seen in **Figure 3**, the substrate is placed on the bottom of a centrifugation vial, with the colloidal solution poured on top. During the centrifugation, the particles deposit on the bottom of the vial, coating the substrate<sup>[14]</sup>.

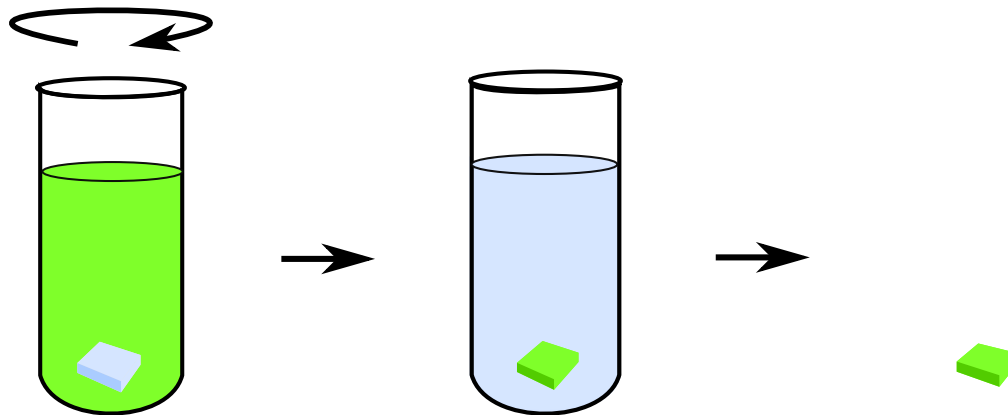


**Figure 3:** Schematic depiction of the centrifugal casting method used to prepare thin films from PNPs.

Additionally, the choice of solvent for both the precursor as well as the precipitation is of vital importance. Perovskites are soluble in polar, aprotic solvents such as dimethylformamide (DMF) and dimethyl sulfoxide (DMSO). However, PNPs prepared from precursors containing DMSO showed an emission maximum at higher wavelengths and a diminished PLQY. This has been attributed to a retarded crystallization process during precipitation. As DMSO coordinatively binds to the lead precursor, the capping agents cannot affect the crystal growth or stabilize the PNPs. This has not been observed when working with precursors containing DMF, which has therefore been almost universally selected for the preparation of PNPs. Similarly, variation in precipitation medium did not show any favorable results for chloroform, diethylether, chlorobenzene or xylene, with highest PQLY values observed when using toluene<sup>[15]</sup>.

Perovskites generally show low stability and are highly affected by ambient conditions such as high temperatures, illumination, oxidizing agents and especially water. Water molecules are able to permeate the crystal structure of the perovskites, forming monohydrates and dihydrates. Furthermore, water can form strong hydrogen bonds with the organic components of the structure, weakening the bonds within the crystal lattices. This increases the susceptibility of the perovskites to further external stressors such as heat<sup>[16]</sup>. However, trace amounts of water are also able to positively influence the formation of the perovskite structure, as they solubilize the precursors in the solvent and provide them with higher mobility. This consequently results in a “healing” effect of the structure, as excess ammonium salt within the solution is removed and therefore, traps within the structure are decreased<sup>[17]</sup>.

It has also been reported, that weak bonding between trace amounts of water and the ammonium group of *t*-*boc*-lysine results in a highly mobile species and thus, in a more efficient surface coverage and therefore smaller nanoparticles emitting at a lower wavelength. If the amount of water is further increased, a shift to higher wavelengths is detected as further complexes are hydrated, the aforementioned “healing” comes to pass, and larger crystallites

are formed. Therefore, water can be used to fine tune the size of PNPs, from precursors without any water showing PNPs with an average size of 4.6 nm, to precursors with 32 mol. equiv. water showing an average size of 6.2 nm<sup>[18]</sup>.

## 1.2. Quantum Confinement

One result of Schrödinger's equation is the definition of quantum numbers and hence the quantization of energy with the consequence that electrons may only occupy certain discrete energy levels. With the convergence atoms and the formation of a crystal lattice, those discrete energy levels merge and form a band of possible energy levels. The strength of the bond holding the electrons to their atomic core of origin determines the width of these bands. The valence electrons which are located in the highest occupied band, the valence band, are more loosely bound to the atomic core and can therefore easily move within the crystal lattice as the valence bands broaden and converge.

In an isolating material, the valence band and the above positioned conduction band are separated by a band gap, which is hardly surpassed by electrons. If no gap is present, with unoccupied levels so close to the valence band, barely any energy is required to promote the uppermost electrons. This increased mobility encourages electrical conductivity, with these materials being classified as conductors<sup>[19]</sup>, as can be seen in **Figure 4**.

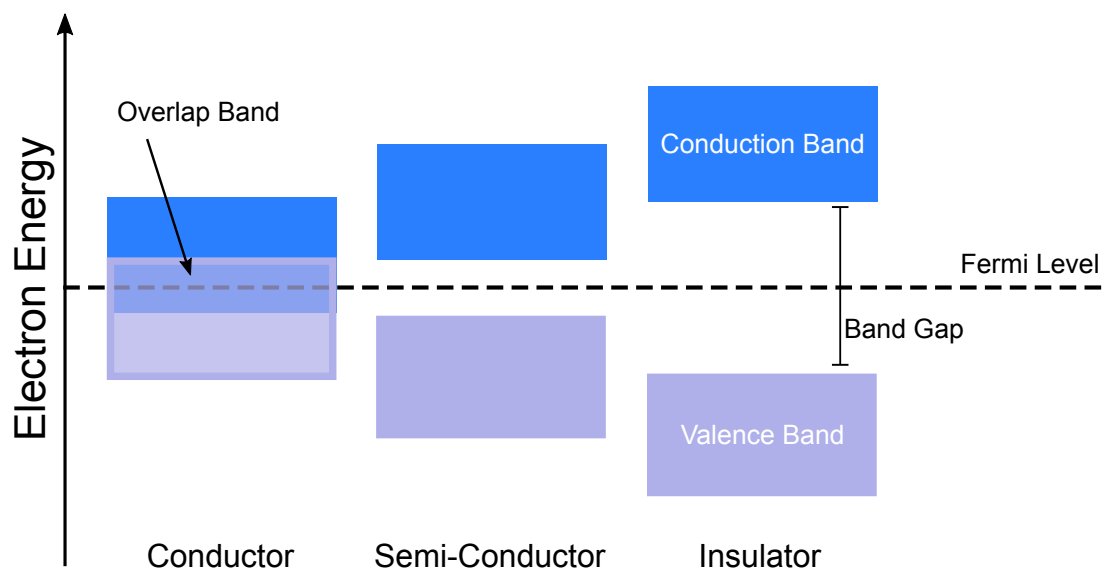


**Figure 4:** Depiction of valence and conduction band of a conductor, semiconductor and insulator.

In some materials a band gap is present between the valence and conduction band. However, with excitation some electrons are able to leave the valence band, cross the band gap and populate the conduction band, leaving behind a positively charged electron hole in the valence band. Both the electron in the conduction band as well as the hole in the valence band are mobile and give rise to electrical conductivity, which rises with increasing temperature

as more electron-hole pairs are created. These materials are classified as semiconductors. As the divide between semiconductor and insulator is not a sharply defined one, but rather a continuous distinction, some definitions have been made using the specific conductivity of materials, with values for semiconductors between  $10^{-8}$  to  $10^4$  S cm<sup>-1</sup> [20,21].

When decreasing the size of semiconductors to nanoscale, their optical as well as electrical properties change substantially. In perovskites some of these changes can be attributed to the quantum confinement effect, which occurs when the size of a nanoparticle becomes so small, it is in a comparable magnitude to the exciton Bohr radius<sup>[22]</sup>. When an electron is excited to the conduction band, it is still bound by coulomb attraction to the electron hole in the valence band. This is called “exciton”, with the exciton Bohr radius describing the space occupied by the exciton. This radius depends on the effective masses of the electron and electron-hole and therefore on the material itself. In bulk materials, the band gap remains at a consistent level. When moving from bulk semiconductors to the nanoscale, the movement of the exciton is hindered and its energy becomes defined by this confinement, as illustrated in **Figure 5**. Furthermore, the size of the band gap is affected by this confinement on the nanoscale, typically at sizes below 10 nm. As the size of the nanoparticle decreases, the band gap increases, with the energy levels at the band edges becoming more discrete<sup>[23,24]</sup>. Therefore more energy is needed to create an exciton, shifting the emission of the nanoparticle to a lower wavelength and bluer colour, which is called a hypsochromic shift.

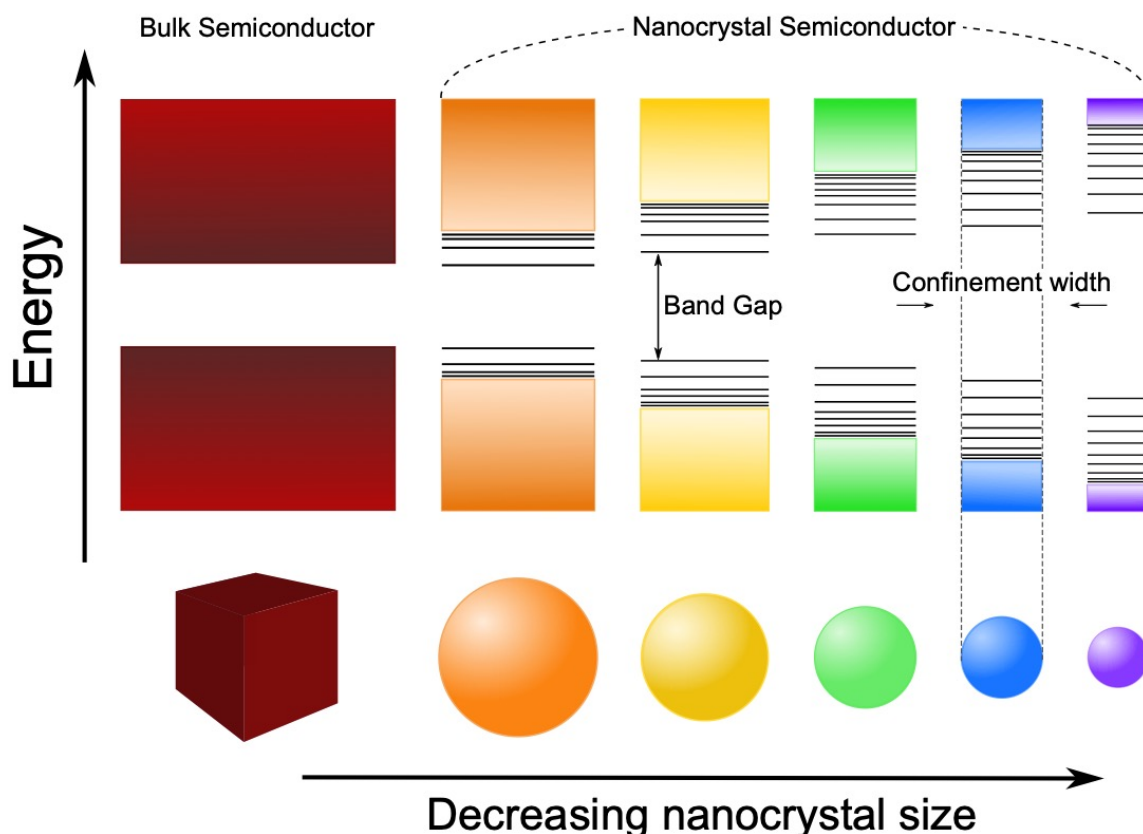


**Figure 5:** Schematic depiction of quantum confinement effect.

### 1.3. Photoluminescence

In photoluminescence light is emitted after the previous absorption of a photon. The surplus of energy after the photoexcitation is released by different relaxation processes, most commonly by the reemittance of a photon.

When exciting a semiconductor, a photon with a higher energy than the band gap is absorbed, creating an electron-hole pair. This excited electron decreases in energy due to various relaxation processes until reaching the edge of the conduction band. Here, the electron and hole recombine, releasing a photon in a process called radiative recombination. An important measure for characterizing photoluminescent substances is the photoluminescence quantum yield (PLQY), which is given by the ratio of number of emitted photons to the number of absorbed photons.

However, not all electron-hole pairs recombine radiatively. Within the semiconductor, trap-states can form, often caused by lattice defects, such as missing atoms, chemical impurities, etc. Those trap states form states within the band gap, therefore lying below the conduction band, yet above the valence band. Electron-hole pairs tend to move to those trap states and recombine there. This recombination is often in the form of heat dissipation, therefore being non-radiatively and diminishing the PLQY. Another form of trap states are surface traps. These originate from undercoordinated surface ligands and also form states within the band gap. Compared to bulk material, nanoparticles have a high surface to volume ratio and which is why they are more susceptible to surface traps<sup>[25]</sup>. In perovskite nanoparticle structures, those surface traps are avoided by using a ligand assisted precipitation method as already described above<sup>[11]</sup>.

## 2. Experimental

### 2.1. Precursor Solutions

If not stated otherwise, the precursors were prepared in the ratio reported in this section which was adapted from the general procedure described by Prochazkova *et al.*<sup>[18]</sup>. The organic compound (0.038 mmol, 1.1 equiv.) being either methylammonium bromide (MABr) or formamidinium bromide (FABr), as well as *t*-boc-lysine (6.7 mg, 0.027 mmol, 0.8 equiv.) was weighed into a 4 mL vial inside a nitrogen filled glove box. A 340 mM solution of lead bromide (PbBr<sub>2</sub>) was prepared by dissolving PbBr<sub>2</sub> (62.5 mg) in dry dimethyl formamide (DMF, 500  $\mu$ L) of which 100  $\mu$ L (0.034 mmol) were added to the glass vial, with a subsequent addition of HeA (40  $\mu$ L, 0.320 mmol, 9.4 equiv.). Following this, anhydrous DMF (1.15 mL) containing the respective additive listed in **Table 1** below was added to the solution. The precursors were left to stir in the fume hood for at least one day.

**Table 1:** Additives to the dry DMF used for the precursor solutions.

Substance	Molar ratio*	$V_{\text{in 5 mL DMF}} / \mu\text{L}$
Water (18 M $\Omega$ )	8	22
	16	44
	32	88
Methanol	16	94

\* with respect to PbBr<sub>2</sub>

## 2.2. Thin Films

In order to precipitate the perovskite nanoparticles (PNPs), toluene (25 mL) was cooled to 5 °C using an ice bath with the precursor solution (125  $\mu\text{L}$ ) being added while vigorously stirring. The solution was put under vacuum and left to stir for an hour after which the ice bath was removed. A glass slide (1  $\times$  1 cm) was pre-treated using a plasma etch and shortly afterwards put at the bottom of a centrifugation tube. The solution containing the PNPs was poured on top and put into a centrifuge at 5000 rpm for 5 min. The supernatant was removed using a pipette, the films were rinsed with extra toluene and subsequently dried under a toluene atmosphere.

## 2.3. Colloidal Solutions

Similar to the preparation of the thin films, toluene (10 mL) was cooled to 5 °C using an ice bath and the precursor solution (50  $\mu\text{L}$ ) was added while vigorously stirring. The solution was put under vacuum and left to stir for one hour, after which the ice bath was removed, and the solution was poured into a centrifugation tube. The solution was put into the centrifuge at 5000 rpm for 5 min and the supernatant was discarded. The resulting nanoparticles were redispersed in toluene (1 mL) using an ultrasonic bath.

# 3. Results and Discussion

## 3.1. Organic Component

The PNPs were prepared in two different compositions, with the organic compound varying between MABr as well as FABr, which are shown in **Figure 6**. As expected, due to the differently sized organic component, films prepared from MAPbBr<sub>3</sub> particles showed a blue emission with an emission maximum of around 516 nm, while films prepared from FAPbBr<sub>3</sub> particles showed a greener emission at roughly 536 nm.

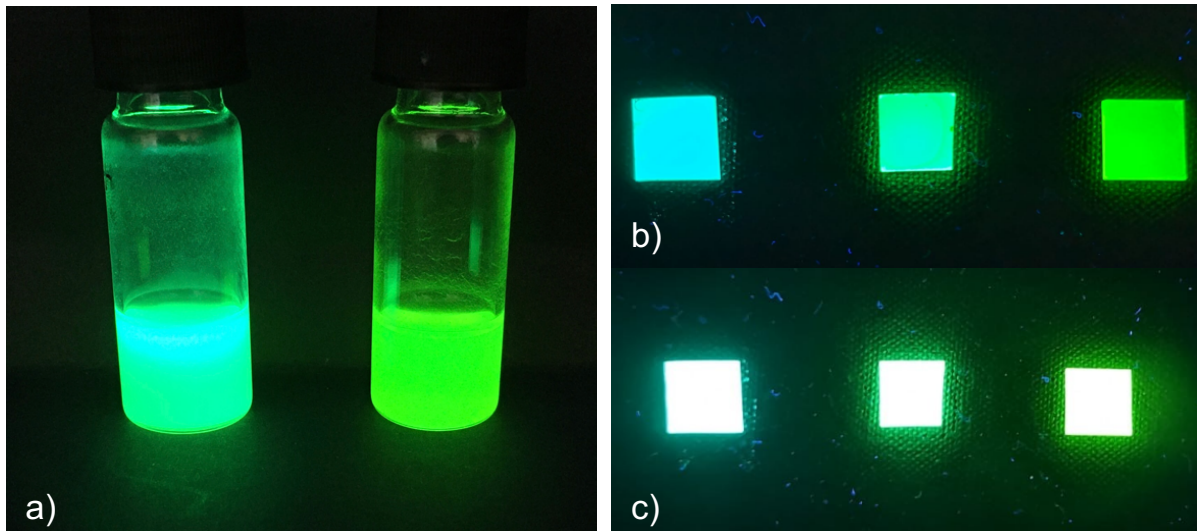


**Figure 6:** Comparison of methyl ammonium bromide and formamidinium bromide a) colloidal solutions (left: MAPbBr<sub>3</sub>, right: FAPbBr<sub>3</sub>) and b - c) thin films under a UV-light source (left to right: MAPbBr<sub>3</sub> with 16 mol. equiv. H<sub>2</sub>O, MAPbBr<sub>3</sub> with 32 mol. equiv. H<sub>2</sub>O and FAPbBr<sub>3</sub> with 16 mol. equiv. H<sub>2</sub>O).

When comparing PLQY of PNPs with different compositions, both perovskite structures showed the potential for extremely high PLQY values. However, values close to 100% were much more frequently observed when preparing FAPbBr<sub>3</sub> thin films, with intermittent values below 97%. In comparison, MAPbBr<sub>3</sub> films averaged 97% PLQY with only the occasional films surpassing this threshold.

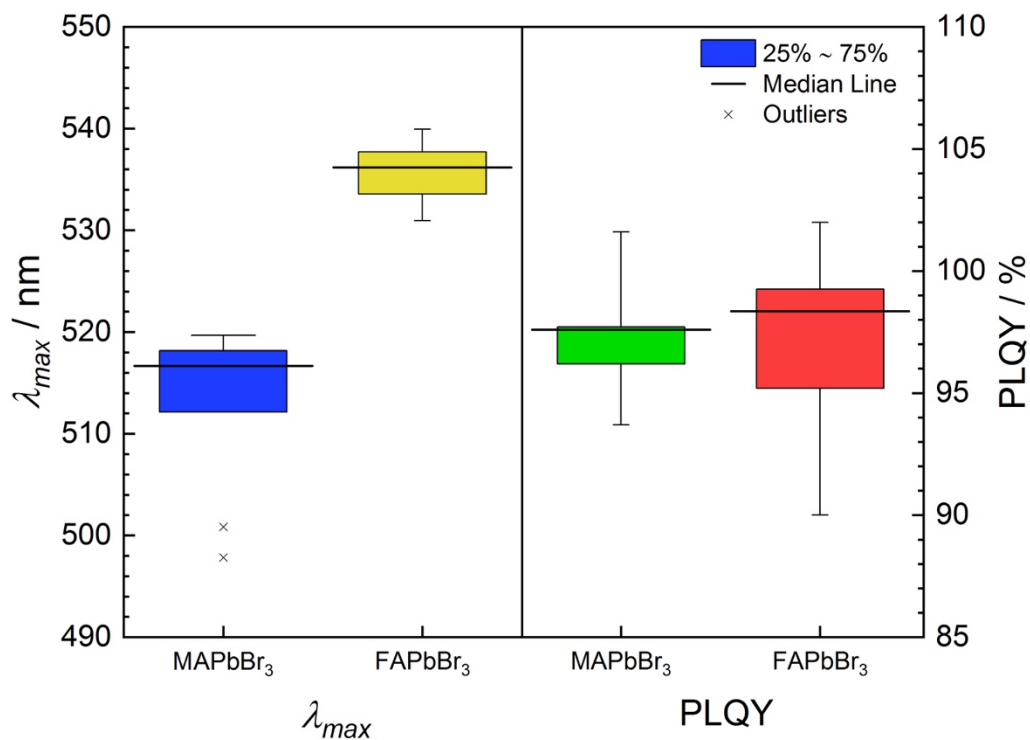


**Figure 7:** Emission maximum as well as PLQY of PNPs prepared with different organic cations.

As depicted in **Figure 7**, both compositions showed an emission maximum in a consistent range when prepared in accordance with the experimental section. However, the emission of MAPbBr<sub>3</sub> nanoparticles showed a much higher dependence on the exact composition of the precursor solution as shown in **Figure 8b**, where an increase in 10 w% of MABr increased the emission maximum by 6 nm (0.035 eV). Larger increases of 40 w% MABr shifted the emission maximum even further, increasing it by a value of 26 nm. Yet, such a large surplus of MABr severely impacted the stability of the PNPs as well as the quantum yield.

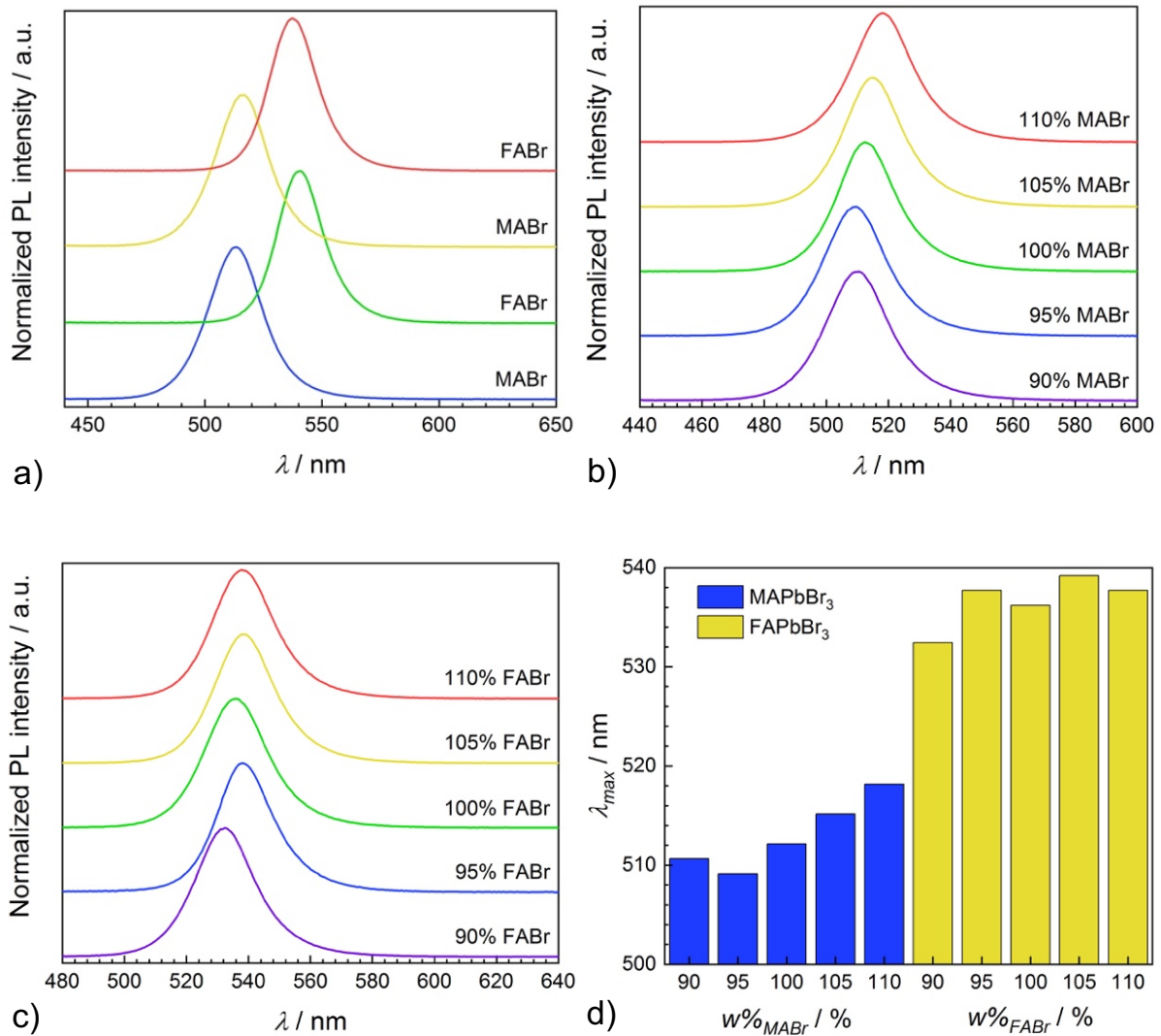


**Figure 8:** a) Comparison of methyl ammonium bromide and formamidinium bromide as organic component of the perovskite structure with b - c) emission spectrum of PNPs with different w% of the organic compound and d) emission maximum against w% of the organic compounds.

In comparison, FAPbBr<sub>3</sub> nanoparticles showed less dependence on the exact composition of the precursor solution, with no significant shift detectable upon alternating the ratio within the precursor, which is shown in **Figure 8c**.

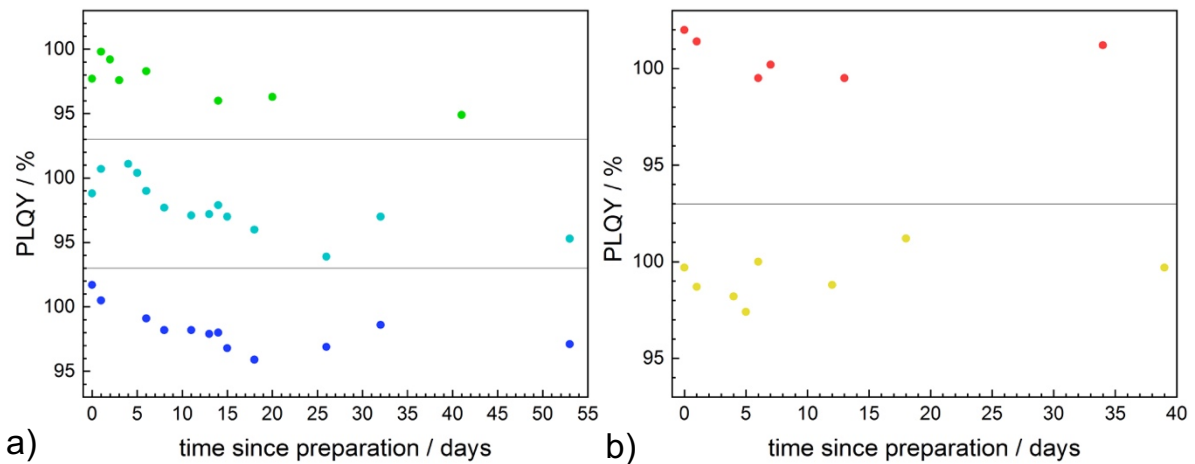


**Figure 9:** Change of PLQY with time since preparation of a) three different MAPbBr<sub>3</sub> films and b) two different FAPbBr<sub>3</sub> films.

Both compositions of PNPs showed instabilities with PLQY values, with high losses commonly observed during the first month. However, the films depicted in **Figure 9a** and **9b** seem to be relatively stable, with minimal losses. As the error for the conducted measurement when measuring highly emissive particles is approximately  $\pm 1.3\%$  and the changes in PLQY only barely exceed this range a definite conclusion is hard to make, aside from the fact that the films in **Figure 9a** seemed to degrade a bit quicker than the films depicted in **Figure 9b**. The film depicted in the lower half of **Figure 9b** even seemed to slightly increase in PLQY. Yet, the films in **Figure 9b** have also not been observed as long as the films depicted in **Figure 9a**. No significant difference in degradation could be noticed upon storing the films differently, neither under vacuum nor in a glove box. Also revitalizing the films by immersing them in a solution of HeA and boc-lysine was not successful, as no change in PLQY could be measured, even upon introducing a film in the solution for up to 40 minutes.

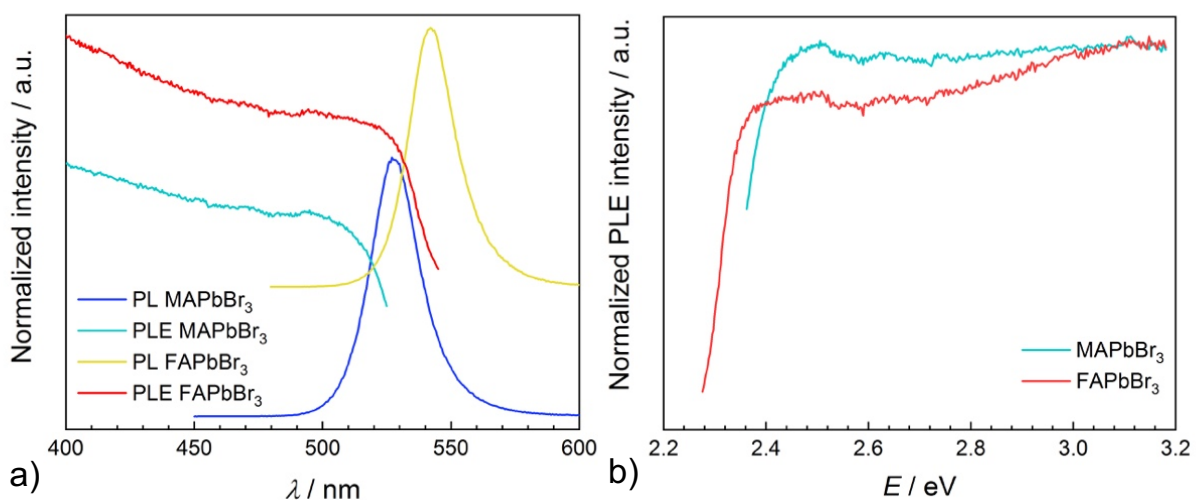


**Figure 10:** a) Photoluminescence emission (PL) and excitation spectra (PLE) of MAPbBr<sub>3</sub> and FAPbBr<sub>3</sub> thin films and b) photoluminescence excitation spectra in dependence of the energy.

When observing the photoluminescence excitation spectra of the two different PNPs depicted in **Figure 10** it can be seen that both compositions of nanoparticles roughly followed the same route. As expected  $\text{FAPbBr}_3$  nanoparticles absorbed in a slightly lower energy region than  $\text{MAPbBr}_3$ , which accounts for these nanoparticles appearing slightly greener in colour.

Moreover, the surface aspect of the thin films was checked by using a profilometer and an optical microscope, which is pictured in **Figure 11**. Both nanoparticle compositions lead to thin films with a rough, uneven surface whereby thin films consisting of  $\text{FAPbBr}_3$  showed a much more uneven surface. Furthermore, those films were significantly thinner when compared to  $\text{MAPbBr}_3$  films. Yet, as both films showed large variation within the surface level, film thickness was hard to quantify, with  $\text{MAPbBr}_3$  thin films being roughly 1200 nm and  $\text{FAPbBr}_3$  thin films being roughly 600 nm in thickness.

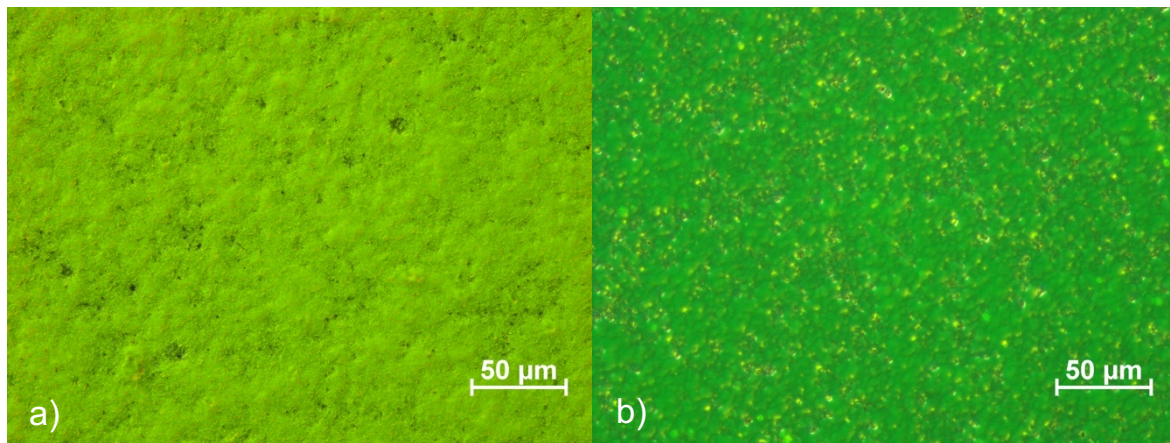


**Figure 11:** Microscopic image of the surface of a)  $\text{MAPbBr}_3$  and b)  $\text{FAPbBr}_3$  thin films.

## 3.2. Water Content

A main focus of this work has been the addition of small amounts of water to the precursor solution in order to manipulate the size<sup>[18]</sup> and emission maximum of the formed nanoparticles. A controlled amount of water introduced during the formation of the nanoparticles can positively influence the crystallization of the perovskite structure<sup>[26]</sup> and enhance PLQY. Yet too high quantities of water irreversibly destroy the PNPs and therefore also lower the PLQYs.

### 3.2.1. Additive to Precursor

As can be seen in **Figure 12a** below, nanoparticles consisting of  $\text{MAPbBr}_3$  showed a clear trend with respect to the increasing addition of water, shifting the emission maximum 10 nm from 8 mol. equiv. of water to 32 mol. equiv. All three compositions showed a PLQY of around 100%, which could no longer be reliably distinguished in-between.

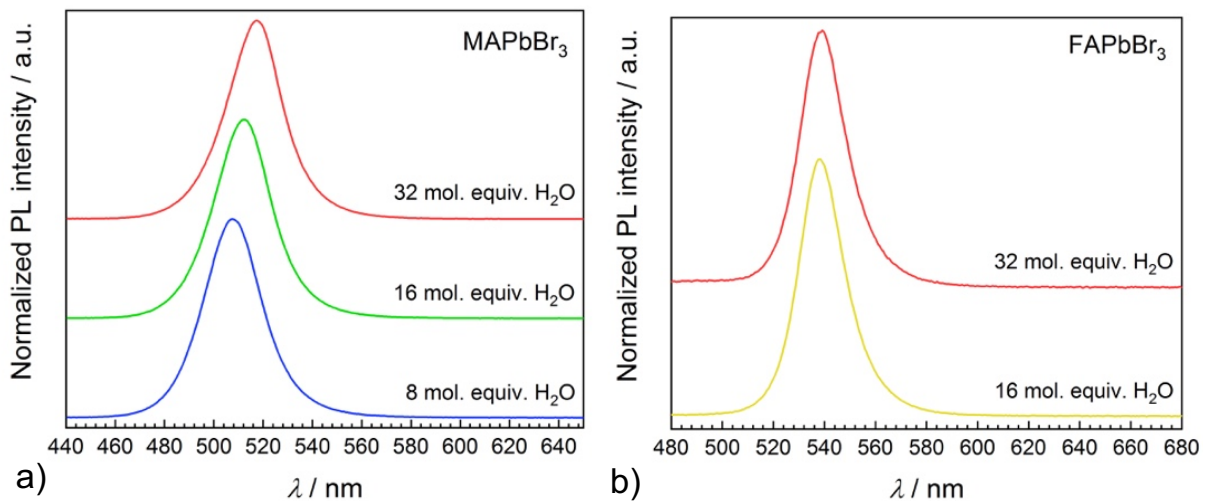


**Figure 12:** Photoluminescence spectrum of a) MAPbBr<sub>3</sub> and b) FAPbBr<sub>3</sub> nanoparticles with varying water content within the precursor solution.

Contrary to the behaviour of MAPbBr<sub>3</sub>, the films prepared from FAPbBr<sub>3</sub> showed no discernable shift in emission maximum, which is illustrated in **Figure 12b**. In addition, the film containing 32 mol. equiv. of water showed a substantially diminished PLQY of around 60%. Therefore, if not explicitly stated otherwise, all precursors within this thesis of both MAPbBr<sub>3</sub> as well as FAPbBr<sub>3</sub> were prepared with 16 mol. equiv. of water.

### 3.2.2. Ambient Humidity

It stands to reason that in addition to the water content within the precursor all other sources of water need to be considered as well. As precipitation of the particles occurred within a fume hood, ambient humidity played a not insignificant part. Yet due to the aging of the precursor solutions this component is rather difficult to quantify. **Figure 13** represents two different films which were prepared twice on the same day, once in the morning as well as once in the afternoon. These films showed vastly different photoluminescence spectra, with a shift in emission maximum of up to 20 nm (0.10 eV). During this time the ambient humidity dropped from 60% to 50%, decreasing the amount of water during the precipitation and shifting the emission to a lower wavelength and higher energy.

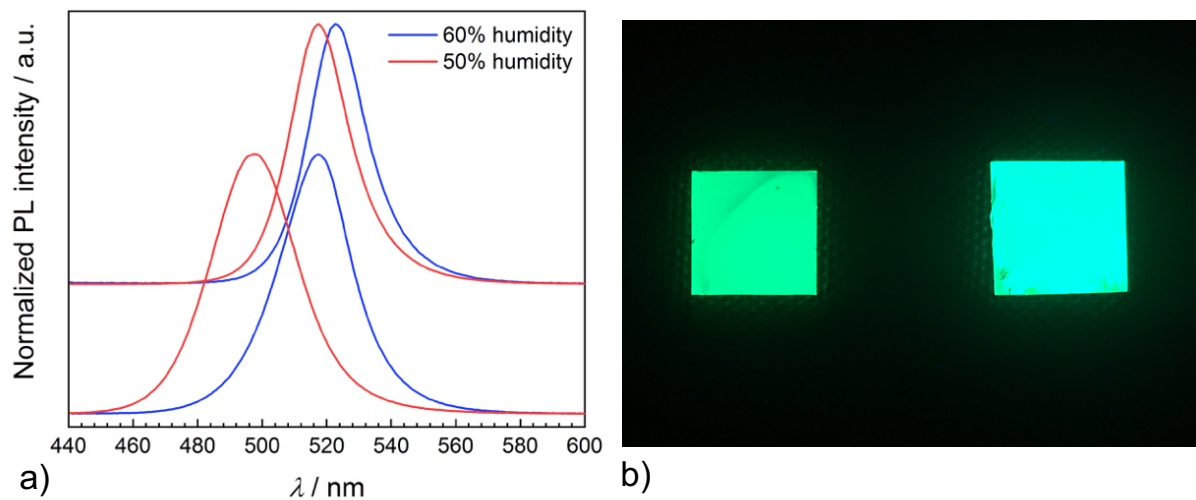


**Figure 13:** a) Photoluminescence spectrum of MAPbBr<sub>3</sub> PNPs at different ambient humidity levels and b) picture of PNP films at different ambient humidity levels under UV-light (left: prepared in the morning at 60% humidity, right: prepared in the afternoon at 50% humidity).

Given the unpredictable nature of perovskites formation, the observed phenomenon is both hard to recreate as well as hard to relate to changes due to ambient humidity. However, whenever working with PNPs, especially based on MAPbBr<sub>3</sub> as those have proven to be more susceptible so changes in water content, observation of humidity levels is not to be neglected.

### 3.2.3. Solvent

An additional source of water within this procedure stems from dissolved water within the toluene used for precipitating the PNPs. A remarkable difference could be seen when switching from one toluene bottle to another, freshly opened one, both in emission maximum as well PLQY. Two different bottles of toluene were examined more thoroughly with the first toluene (toluene<sub>#1</sub>) being a newly opened bottle and the second one (toluene<sub>#2</sub>) being already opened and stored under ambient conditions for some time.

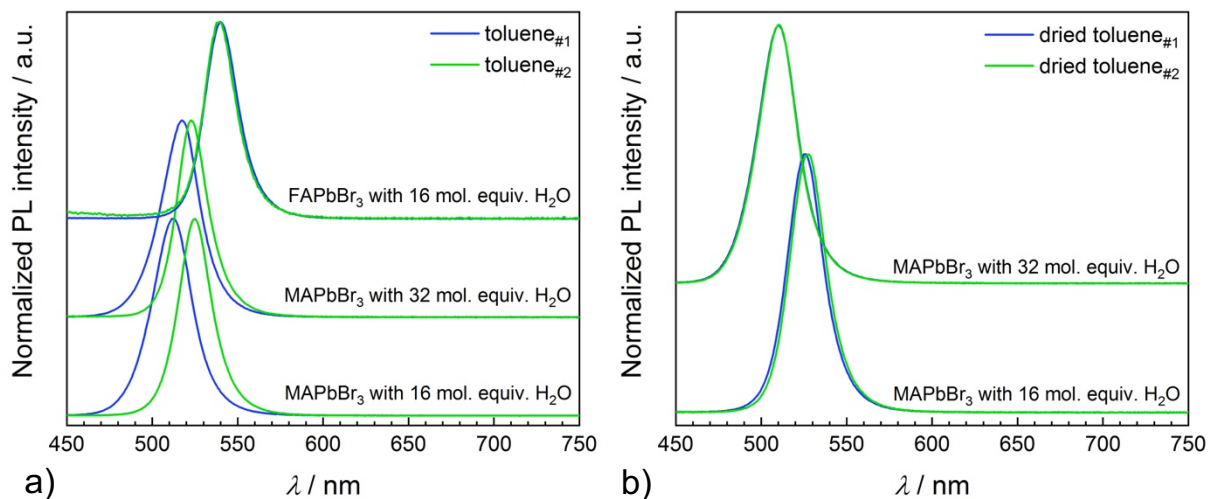


**Figure 14:** Photoluminescence spectrum of PNPs using a) two different toluenes and b) the same toluenes which were previously dried using molecular sieve.

As can be seen in **Figure 14a**, when examining nanoparticles composing of  $\text{MAPbBr}_3$  the use of a different toluene shifted the emission maximum up to 12 nm (0.06 eV). In the case of nanoparticles containing 16 mol. equiv. of water no significant change in the PLQY could be detected, however the PLQY of the nanoparticles containing 32 mol. equiv. of water decreased drastically by around 30%. As has been reported before<sup>[18]</sup>, a water content above 32 mol. equiv. decreases both the PLQY as well as the particle size and likely degrades the perovskite structure. Furthermore, both solvents have been dried using 3 Å molecular sieves. Those dried solvents showed no considerable difference in either emission maximum or PLQY, as can be seen in **Figure 14b**, supporting the assumption of different water content within the solvents.

Additionally, when preparing  $\text{FAPbBr}_3$  nanoparticles no shift in the photoluminescence could be detected upon changing the solvents. However,  $\text{FAPbBr}_3$  prepared with toluene#2 showed a substantially decreased PLQY. This supports the assumption already reported in the section above, that nanoparticles of this composition tolerate less amount of water than nanoparticles composed of  $\text{MAPbBr}_3$ . If not stated otherwise, all nanoparticles within this thesis were prepared using toluene#1.

### 3.3. Methanol Addition to Precursor Solution

In order to investigate further possibilities of hydrogen containing solvents in comparison with water, 16 mol. equiv. of dry methanol (MeOH) have been added to a precursor solution of  $\text{MAPbBr}_3$ . For the sake of comparison, a second solution was prepared containing 16 mol. equiv. of water.

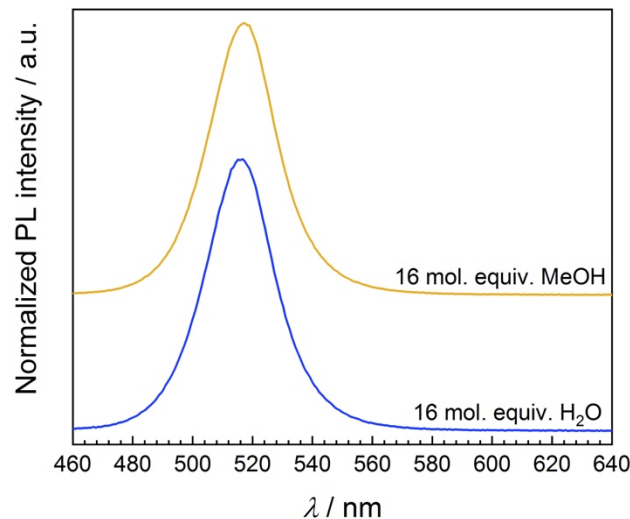


**Figure 15:** Comparison of PNPs made from precursor solutions with 16 mol. equiv. water and 16 mol. equiv. MeOH.

As depicted in **Figure 15**, no noteworthy differences could be detected between the two samples in either emission maximum, PLQY or longevity. Therefore, it stands to reason that MeOH is equally as capable as water in mobilizing the ligands and deploying a healing effect to the perovskite structure. However, further experiments would have to be conducted in order to verify this conclusion.

### 3.4. Age of Precursor

According to the procedure adapted from Prochazkova *et al.*<sup>[18]</sup>, the precursor solutions for preparing MAPbBr<sub>3</sub> nanoparticles were left to stir for up to 7 days. During this time, the initially turbid solution cleared to a totally transparent one. This behaviour was accelerated with increasing water content within the precursor.

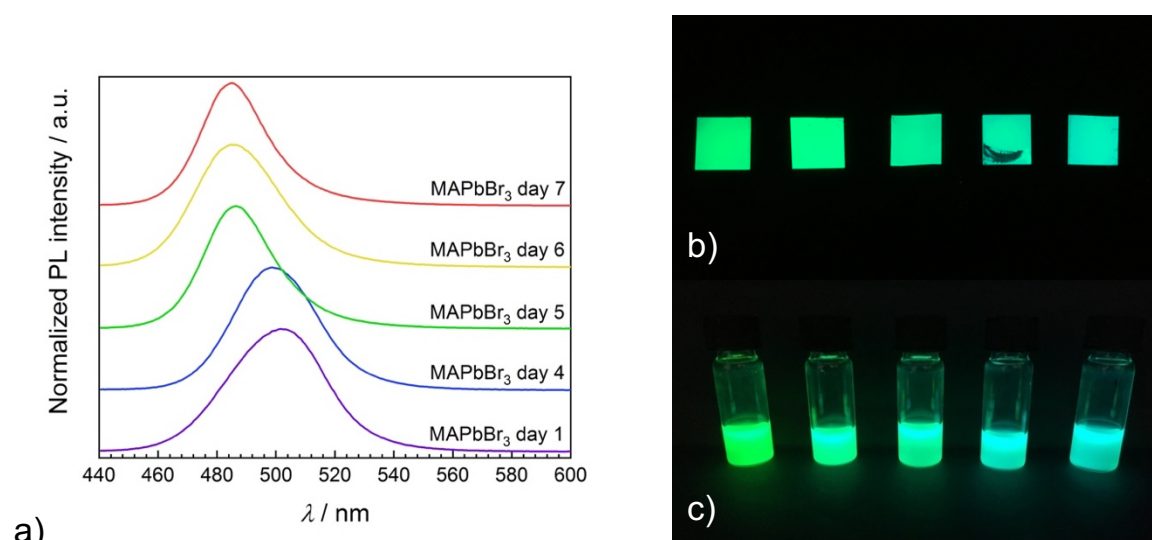


**Figure 16:** a) Photoluminescence spectrum of PNPs prepared from differently aged MAPbBr<sub>3</sub> precursor solutions, b) thin films and c) colloidal solutions prepared from the same precursors (from left to right: 1, 4, 5, 6 and 7 day old precursor solution).

However, when using aged precursors older than two days, a noticeable shift to a higher energy emission was detected, which can be seen in **Figure 16**. This shift occurred in accordance with a decrease in PLQY, dropping to values lower than 90%, with highest PLQYs being achieved using precursors which were prepared the preceding day. Therefore, if not stated otherwise, all films discussed in this thesis were prepared on the day immediately after preparation of the precursor solution.

Precursor solutions for preparation of FAPbBr<sub>3</sub> nanoparticles never turned turbid and cleared immediately after all the initial components were dissolved. No satisfying results could be achieved when using precursor solutions aged more than one day. PLQY of 80% were obtained when storing the solutions in the glove box and even lower quantum yields for previously opened solutions. Therefore all FAPbBr<sub>3</sub> nanoparticles were prepared within 24 h after the preparation of the associated precursor solution.

### 3.5. Low Temperature Spectroscopy

Using low temperature spectroscopy, information about the charge carrier mobility within a semiconductor can be acquired. At room temperature, the shape of the photoluminescence spectrum of the PNPs is mostly defined by the recombination of an exciton, but is also influenced by the size distribution, trap states as well as exciton-phonon interactions. At low temperatures, charge carriers within the semiconductor are randomly frozen in energy states, decreasing the effects of intrinsic scattering based on exciton-phonon interactions<sup>[27]</sup>.

The following PNP thin films were both measured on the day after their production from 4 K to 295 K.

#### 3.5.1. MAPbBr<sub>3</sub> Thin Film

As seen in **Figure 17a**, when cooling the MAPbBr<sub>3</sub> film to 4 K, the emission maximum decreased in intensity and shifted to a higher wavelength which correlates to a lower energy of 2.28 eV. Upon the subsequent heating, the emission stayed in this higher wavelength, lower energy region only up to 10 K. Afterwards the energy maximum gradually increased until 170 K, where at 2.35 eV the increase slightly levelled off. At this point, the peak shape of the emission changed, as can be seen in **Figure 17b**. The initially narrow and symmetric shape showed a slight peak broadening at the lower energy side of the spectrum, which persisted until room temperature was reached. Interestingly, as can be seen in **Figure 17c**, the maximum peak energy decreased to 2.35 eV, which was last reached at 170 K. This decrease upon reaching room temperature has also been reported in literature<sup>[28,29]</sup>, however not in this magnitude. Given that the experiment was only carried out once with one PNP thin film, it is still unclear whether the prominence of this decrease is an intrinsic property of the material, or a coincidence within this measurement.

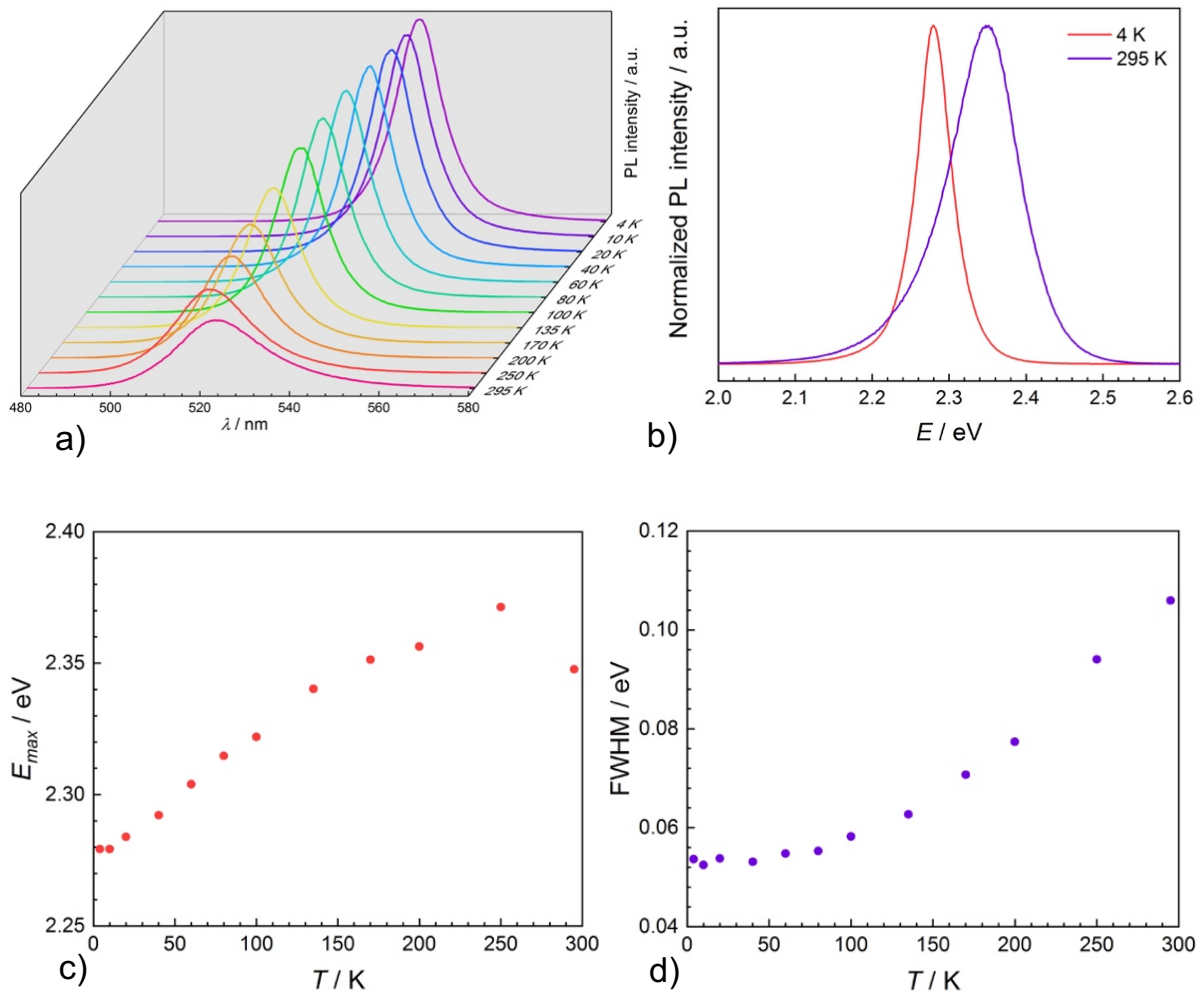


**Figure 17:** Low temperature spectroscopy of a MAPbBr<sub>3</sub> thin film with a) individual photoluminescence spectra, b) depiction of the shape difference of the photoluminescence spectrum at 4 and 295 K, c) peak energy and d) full width at half maxima as a function of the temperature.

When observing the full width at half maxima (FWHM), at low temperatures the spectrum stayed at a mostly consistent 0.05 eV until reaching 100 K, as seen in **Figure 17d**. Here the value gradually increased from 0.05 eV until reaching 0.11 eV at room temperature. In PNPs, the FWHM is largely dependent on the size distribution of the nanoparticles. Yet this temperature dependent increase suggests that the aforementioned exciton-phonon interactions also contribute to the broadening of the peak<sup>[27,30]</sup>.

Interestingly, semiconductors normally show a red shift of their emission upon increasing temperature, decreasing the band gap due to electron-phonon interactions<sup>[31]</sup>. In perovskites however, this trend is in reverse, most likely due to thermal expansion. Here, the crystal lattice is expanded which leads to a decreased interaction between the two valence orbitals. This in turn leads to a lower valence band-width, an increase in the band gap and an emission spectrum shifted to a higher energy region<sup>[32]</sup>. However, this explanation is still speculative and no definitive conclusion has been reached.

### 3.5.2. FAPbBr<sub>3</sub> Thin Film

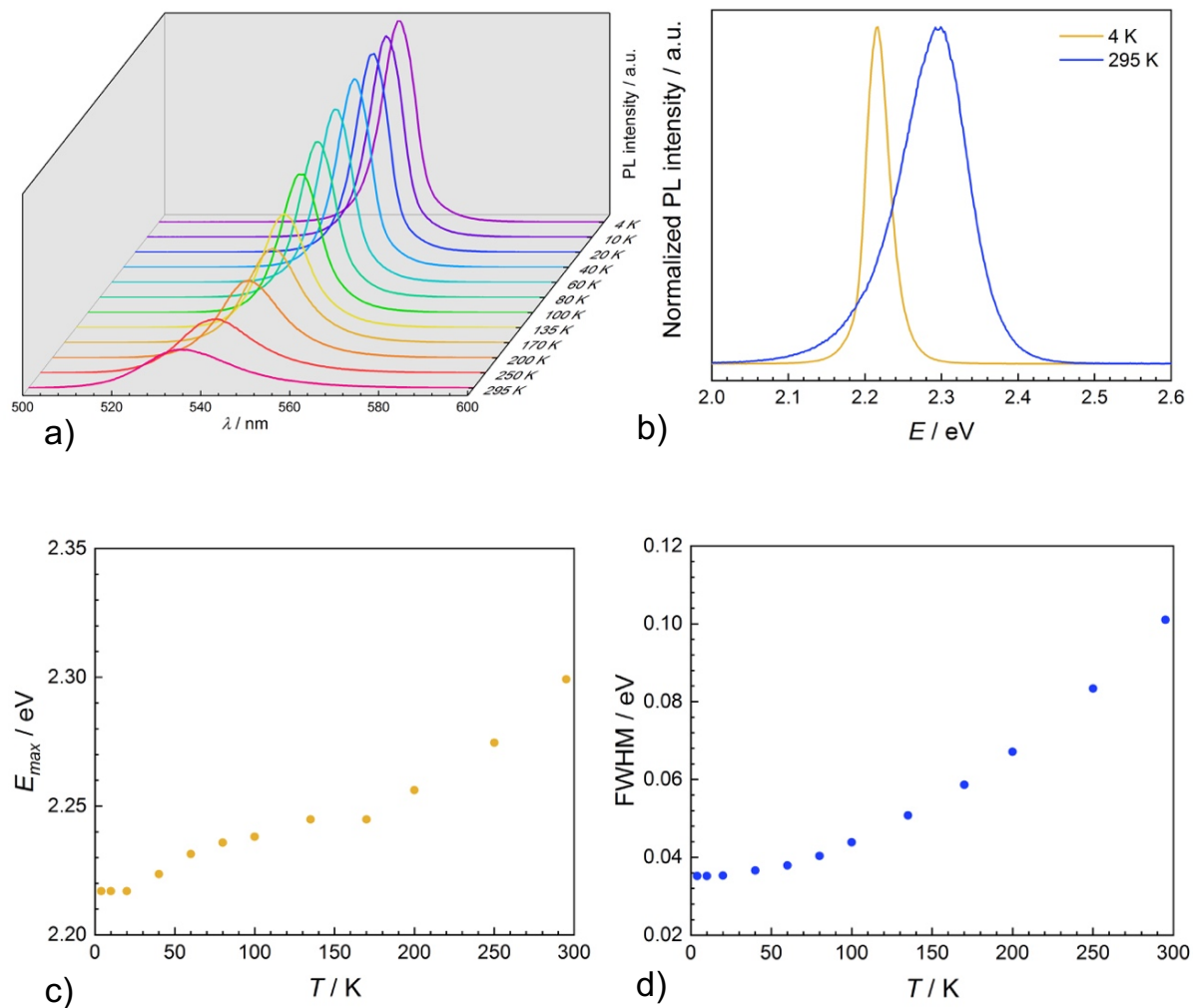


**Figure 18:** Low temperature spectroscopy of a FAPbBr<sub>3</sub> thin film with a) individual photoluminescence spectra, b) depiction of the shape difference of the photoluminescence spectrum at 4 and 295 K, c) peak energy and d) full width at half maxima as a function of the temperature.

The measured FAPbBr<sub>3</sub> thin film behaved in much the same way as the MAPbBr<sub>3</sub> with a decrease in intensity and a shift to higher energies upon temperature increase, as can be seen in **Figure 18a**. Similarly, an asymmetric peak formed upon heating, with peak broadening on the lower energy side of the spectrum (**Figure 18b**) at 200 K.

Yet, when observing FAPbBr<sub>3</sub> no decrease in peak energy upon reaching room temperature could be noted. As seen in **Figure 18c**, after 20 K was passed, the peak energy slowly increased with a more rapid increase upon passing 200 K. Changes in FWHM roughly followed the same course as already discussed with MAPbBr<sub>3</sub>, as illustrated in **Figure 18d**. Although, FAPbBr<sub>3</sub> displayed a much narrower peak at low temperatures with a FWHM of 0.035 eV, the FWHM at room temperature was of a similar size as seen in the MAPbBr<sub>3</sub> thin film. This suggests that the exciton-phonon interactions most likely responsible for this broadening of the peak shape was much more pronounced within FAPbBr<sub>3</sub>. Furthermore, the

FAPbBr<sub>3</sub> thin film which was observed in this experiment seemed to have a much more uniform size distribution, which would explain the narrower peak at 4 K. However, as mentioned before, only one PNP thin film was examined. Therefore, it is unclear, whether this behaviour is an intrinsic property of the material or a mere coincidence during this measurement.

## 4. Conclusion

This thesis aimed to identify different parameters which influence the result of the synthesis of lead bromide PNPs. It has been shown that the water content present during any stage of the synthesis is of vital importance. Especially unintentional water sources in the solvent or under ambient conditions showed to influence the features of the resulting nanoparticles. These results also indicate that in order to reliably control the synthesis for PNPs an exclusion of air and anhydrous solvents would be beneficial. However, no synthesis under those conditions has been conducted in the present thesis, as air was always introduced into the synthesis upon the injection of the precursor solution. Furthermore, the age of the precursor was evidently a significant factor within the synthesis, especially when producing FAPbBr<sub>3</sub> PNPs.

A noticeable challenge during this work was the low stability of the resulting nanoparticles. Especially the thin film samples showed a substantial variation in longevity, ranging from a few days, to a few weeks, to over a month. Further research should therefore focus on improving the stability of the nanoparticles. Additionally, the thin films produced in this thesis showed a highly uneven surface, especially with thin films compositing of FAPbBr<sub>3</sub>. In order for these materials to be applicable, a smoother surface would need to be achieved.

With the synthesis described in this thesis, the production of PNPs with PLQYs of around 100% can be reliably done. This proved to be the case for both nanoparticles compositing of MAPbBr<sub>3</sub> as well as of FAPbBr<sub>3</sub>. Hereby, FAPbBr<sub>3</sub> thin films showed a slightly higher PLQY, however, MAPbBr<sub>3</sub> showed less distribution within the values for PLQYs. These results show great promise for application of these nanoparticles in optoelectronic devices, such as LEDs.

## 5. Appendix

### 5.1. Chemicals

If not stated otherwise all chemicals were used as received.

**Table 2:** Used chemicals.

Chemical	Abbreviation	Molar Mass / g mol <sup>-1</sup>	Purity / %	Vendor
Dimethylformamide	DMF	73.09	99.8	Sigma-Aldrich
Formamidinium bromide	FABr	124.97	–	–
Hexanoic acid	HeA	116.16	> 99	Sigma-Aldrich
Lead bromide	PbBr <sub>2</sub>	367.01	99.99	Sigma-Aldrich
Methanol	MeOH	32.04	99.8	Sigma-Aldrich
Methylammonium bromide	MABr	111.97	–	Greatcell Solar Materials
Molecular Sieves	–	–	–	Alfa Aesar
<i>t</i> - <i>boc</i> -Lysine	–	246.30	97	Alfa Aesar
Toluene	–	92.14	–	VWR

## 5.2. Instruments

**Table 3:** Used instruments.

Instrument	Name and Vendor	Settings
Centrifuge	Scientific Multifuge 1S – Thermo Fischer	5 minutes at 5000 rpm
Integrating-sphere	Hamamatsu Photonics A9924-06 – Hamamatsu	used with L9799-01 continuous mode Xe lamp, a C8849 lamp power supply, a A10080-01 monochromator and a PMA- 12 photonic multi-channel analyser at an excitation wavelength of 405 nm
Low Temperature Spectroscopy	Optistat Dry BLV – Oxford Instruments	excited at $\lambda = 405$ nm with OBIS Coherent continuous wave lasers with Shamrock spectrometer SR-303i-A equipped with an intensified charge coupled device camera (Andor iStar DH320T-18U-73) used for detection
Optic Microscope	Eclipse LV100ND – Nikon	used with dark field mode and an external light source
Plasma Cleaner	PE-25 – Plasma Etch Inc.	equipped with a JB Industries Inc. DV- 142N - Platinum 5 CFM vacuum pump, used with O <sub>2</sub> gas, at 100 W for 5 min
Profilometer	DektakXT – Bruker	
Ultrapure water system	Arium mini plus – Sartorius	–
Ultrasonic bath	VWR Ultrasonic Cleaner	–

---

– VWR Chemicals

UV-Vis spectro- fluorometer	QuantaMaster 40 – PTI	equipped with two monochromators on both the excitation and emission channels
--------------------------------	-----------------------	---

---

## 6. Literature

- [1] Y. Gao, Y. Wu, H. Lu, C. Chen, Y. Liu, X. Bai, L. Yang, W. W. Yu, Q. Dai, Y. Zhang, *Nano Energy* **2019**, *59*, 517.
- [2] J. Li, Y. Shen, Y. Liu, F. Shi, X. Ren, T. Niu, K. Zhao, S. F. Liu, *ACS Applied Materials and Interfaces* **2017**, *9*, 19176.
- [3] X. Zhu, Y. Lin, Y. Sun, M. C. Beard, Y. Yan, *Journal of the American Chemical Society* **2019**, *141*, 733.
- [4] G. Li, Z. K. Tan, D. Di, M. L. Lai, L. Jiang, J. H. W. Lim, R. H. Friend, N. C. Greenham, *Nano Letters* **2015**, *15*, 2640.
- [5] P. Zolfaghari, G. A. de Wijs, R. A. de Groot, *Journal of Physics Condensed Matter* **2013**, *25*, 1.
- [6] S. Gholipour, M. Saliba, *Bandgap Tuning and Compositional Exchange for Lead Halide Perovskite Materials*, Elsevier Inc., **2020**.
- [7] J. M. Frost, K. T. Butler, F. Brivio, C. H. Hendon, M. van Schilfgaarde, A. Walsh, *Nano Letters* **2014**, *14*, 2584.
- [8] T. Sato, S. Takagi, S. Deledda, B. C. Hauback, S. I. Orimo, *Scientific Reports* **2016**, *6*, 1.
- [9] S. C. Tidrow, *Ferroelectrics* **2014**, *470*, 13.
- [10] A. Pan, B. He, X. Fan, Z. Liu, J. J. Urban, A. P. Alivisatos, L. He, Y. Liu, *ACS Nano* **2016**, *10*, 7943.
- [11] S. González-Carrero, L. Martínez-Sarti, M. Sessolo, R. E. Galian, J. Pérez-Prieto, *Journal of Materials Chemistry C* **2018**, *6*, 6771.
- [12] A. Jancik Prochazkova, S. Demchyshyn, C. Yumusak, J. Másilko, O. Brüggemann, M. Weiter, M. Kaltenbrunner, N. S. Sariciftci, J. Krajcovic, Y. Salinas, A. Kovalenko, *ACS Applied Nano Materials* **2019**, *2*, 4267.
- [13] J. Song, J. Li, X. Li, L. Xu, Y. Dong, H. Zeng, *Advanced Materials* **2015**, *27*, 7162.
- [14] S. Gonzalez-Carrero, L. C. Schmidt, I. Rosa-Pardo, L. Martínez-Sarti, M. Sessolo, R. E. Galian, J. Pérez-Prieto, *ACS Omega* **2018**, *3*, 1298.
- [15] A. J. Prochazkova, M. C. Scharber, C. Yumusak, J. Jančík, O. Brüggemann, M. Weiter, N. S. Sariciftci, J. Krajcovic, *Scientific Reports* **2020**, *10*, 15720.
- [16] C. C. Boyd, R. Cheacharoen, T. Leijtens, M. D. McGehee, *Chemical Reviews* **2019**, *119*, 3418.

- [17] C. C. Chueh, C. Y. Liao, F. Zuo, S. T. Williams, P. W. Liang, A. K. Y. Jen, *Journal of Materials Chemistry A* **2015**, 3, 9058.
- [18] A. Jancik Prochazkova, Y. Salinas, C. Yumusak, M. C. Scharber, O. Brüggemann, M. Weiter, N. S. Sariciftci, J. Krajcovic, A. Kovalenko, *ACS Applied Nano Materials* **2020**, 3, 1242.
- [19] N. Mahato, M. O. Ansari, M. H. Cho, *Advanced Materials Research* **2015**, 1116, 1.
- [20] L. Stiny, in *Aktive Elektronische Bauelemente - Aufbau, Struktur, Wirkungsweise, Eigenschaften Und Praktischer Einsatz Diskreter Und Integrierter Halbleiter-Bauteile*, Springer Vieweg, **2016**, pp. 5–38.
- [21] P. Atkins, J. de Paula, *Materials 2: The Solid State*, Oxford University Press, **2006**.
- [22] O. D. Neikov, N. A. Yefimov, in *Handbook of Non-Ferrous Metal Powders*, Elsevier Ltd., **2019**, pp. 271–311.
- [23] J. Orton, in *Semiconductors and the Information Revolution: Magic Crystals That Made IT Happen*, Elsevier B.V., **2009**, pp. 163–192.
- [24] Q. Akkerman, *The Physics behind Semiconductor Nanocrystals*, **2019**.
- [25] M. A. Boles, D. Ling, T. Hyeon, D. v. Talapin, *Nature Materials* **2016**, 15, 364.
- [26] J. Huang, S. Tan, P. D. Lund, H. Zhou, *Energy and Environmental Science* **2017**, 10, 2284.
- [27] L. Turyanska, A. Patanè, M. Henini, B. Hennequin, N. R. Thomas, *Applied Physics Letters* **2007**, 90, 2005.
- [28] H. C. Woo, J. W. Choi, J. Shin, S. H. Chin, M. H. Ann, C. L. Lee, *Journal of Physical Chemistry Letters* **2018**, 9, 4066.
- [29] Y. Liu, H. Lu, J. Niu, H. Zhang, S. Lou, C. Gao, Y. Zhan, X. Zhang, Q. Jin, L. Zheng, *AIP Advances* **2018**, 8, 1.
- [30] M. I. Dar, G. Jacopin, S. Meloni, A. Mattoni, N. Arora, A. Boziki, S. M. Zakeeruddin, U. Rothlisberger, M. Grätzel, *Science Advances* **2016**, 2, 1.
- [31] W. Liu, Y. Zhang, W. Zhai, Y. Wang, T. Zhang, P. Gu, H. Chu, H. Zhang, T. Cui, Y. Wang, J. Zhao, W. W. Yu, *Journal of Physical Chemistry C* **2013**, 117, 19288.
- [32] A. Shinde, R. Gahlaut, S. Mahamuni, *Journal of Physical Chemistry C* **2017**, 121, 14872.